1998

Dynamics of Rydberg States of Nitric Oxide Probed By Two-Color Resonant Four-Wave Mixing Spectroscopy

Elizabeth McCormack
Bryn Mawr College, emccorma@brynmawr.edu

F. Di Teodoro

J. M. Grochocinski

S. T. Pratt

Custom Citation
E.F. McCormack, F. Di Teodoro, J.M. Grochocinski and S.T. Pratt, *J. Chem. Phys.* **109**, 63 (1998).

Dynamics of Rydberg states of nitric oxide probed by two-color resonant four-wave mixing spectroscopy

E. F. McCormack, F. Di Teodoro, and J. M. Grochocinski
Bryn Mawr College, Bryn Mawr, Pennsylvania 19010

S. T. Pratt
Argonne National Laboratory, Argonne, Illinois 60439

(Received 17 February 1998; accepted 25 March 1998)

Two-color resonant four-wave mixing (TC-RFWM) spectroscopy has been used to probe highly excited $v=0$ and $v=1$ Rydberg states of nitric oxide. Transitions to $n=16$–30, $v=0$, Rydberg states, and the $8p$, $9p$, $7f$, $8f$, $8s$, and $9s$, $v=1$ Rydberg states from the $A\ ^2\Sigma^+$, $v'=0$ and 1 states have been recorded. The decay rate of the $8p$ and $9p$, $v=1$ states has been extracted from the observed line profiles by using a recently developed model for the excitation of quasibound resonances in TC-RFWM spectroscopy. Transitions from the $A\ ^2\Sigma^+$, $v'=1$ state to the $X\ ^2\Pi_{3/2}$, $v''=10$ state have also been observed, allowing an absolute calibration of the TC-RFWM signal intensity. This calibration is used to determine an excited-state absorption cross section for the $9p$, $v=1$ Rydberg state. © *1998 American Institute of Physics.* [S0021-9606(98)01625-0]

I. INTRODUCTION

Nitric oxide serves as an important system in which to study the dynamical properties of highly excited Rydberg states of diatomic molecules. Further, the interplay between experimental observations of the Rydberg states of NO using various spectroscopic techniques and multichannel quantum defect theory (MQDT),[1] which provides an integrated approach to describe the dynamics of Rydberg states, has led to significant advances in our understanding of molecular decay mechanisms. The Rydberg series of NO have been studied in detail, beginning with the high resolution vacuum-ultraviolet absorption spectroscopy conducted by Miescher and co-workers.[2–4] Since then many experimental studies using multiphoton excitation techniques have been carried out on highly excited Rydberg states both below[5–12] and above[13–27] the first ionization limit. Remarkably detailed understanding of the photoionization dynamics of these highly excited states has been gained through the use of energy and angle-resolved photoelectron detection.[26–28] The photodissociation dynamics of the highly excited Rydberg states of NO, however, have proven more difficult to measure. What is known about these processes has been gained through the comparison of multiphoton ionization spectra and fluorescence dip spectra,[12–14,27] and direct photofragment detection.[20–22,27] These studies have shown that when both ionization and dissociation channels are open, Rydberg and valence state interactions[29–31] lead to a competition between ionization and dissociation, resulting in Rydberg state widths and profiles that depend strongly on energy and angular momentum. MQDT calculations[32–35] have been successful in describing this competition, and computed cross sections and linewidths are available to make quantitative comparisons.

Two-color resonant four-wave mixing (TC-RFWM) techniques have emerged as effective nonlinear spectroscopic probes and many applications of four-wave mixing techniques to gas-phase molecular spectroscopy have been reviewed.[36,37] Recent work using state-selective TC-RFWM configurations includes the demonstration of a novel slit-jet design that significantly improves signal strengths[38] and new measurements in a variety of molecular systems: O_2,[39] NH_3,[40] pyrazine,[41] benzene,[42] I_2,[43] and H_2O.[44] In NO, TC-RFWM has been used in an investigation of the predissociative linewidths of the $M\ ^2\Sigma^+$, $v=1$ and $H\ ^2\Sigma^+$, $H'\ ^2\Pi$, $v=2$ Rydberg states and the non-Rydberg $B\ ^2\pi$, $v=26$ state;[45] in the determination of energies and rotational constants for several $v=0$ high Rydberg states;[46] and in a study of the multistate interactions between the $B\ ^2\Pi$, $v=28$ and $L\ ^2\Pi$, $v=8$ valence states, and the $Q\ ^2\Pi$, $v=0$ Rydberg state.[47,48]

The TC-RFWM techniques have received attention because they have several valuable attributes. Unlike excited-state detection by the fluorescence-dip method, the RFWM techniques produce a zero-background signal and do not require the state of interest to have a significant fluorescence quantum yield. Although they are inherently not as sensitive as resonance-enhanced multiphoton ionization (REMPI), which, in principle, can detect a single molecule, RFWM techniques probe any absorbing transitions of a molecule, independent of the decay channel, e.g., ionization, dissociation, or fluorescence. In this way, the spectra obtained by using RFWM are directly related to absorption spectra, with the significant advantage of state selection when double-resonance techniques are used. This sensitivity allows efficient detection of states that predissociate or otherwise internally convert their energy, making their detection by other techniques difficult. It is this aspect of the RFWM techniques that makes them particularly well suited to the study of excited-state decay dynamics.

Considerable progress has been made in establishing the relationship between the intensities and linewidths observed in TC-RFWM experiments and those of true excited-state absorption spectra. Theoretical models of TC-RFWM based

on an extension of theoretical work on DFWM[49] that combines diagrammatic perturbation theory with spherical tensor analysis have been developed.[50] This method has been successful in the interpretation of line intensities and line profiles observed in TC-RFWM experiments detecting bound to bound state transitions, where the line profile has been shown to reduce to a simple Lorentzian function of the probe laser frequency.[51] For cases where quasibound states are accessed in the four-wave mixing process, the same approach can be used to derive the appropriate signal intensities and line profiles. In such cases, the line profiles can exhibit pronounced asymmetries reflecting the configuration interaction of the discrete and continuum character of the states.[52]

To demonstrate the utility of TC-RFWM techniques for quantitative studies of the dynamics of Rydberg states and to test the recent theoretical developments, highly excited and quasibound Rydberg states in NO have been investigated. The region just above the ionization threshold is of particular interest because the competition between decay processes leads to transitions that exhibit a variety of line profiles. The region below the first ionization potential is also of interest because the $v=0$ Rydberg states are known to be strongly predissociative and some series have been difficult to observe with ionization detection. Results are presented here on the TC-RFWM spectra of $n=16-30$, $v=0$, Rydberg states and the $8p$, $9p$, $7f$, $8f$, $8s$, and $9s$, $v=1$ Rydberg states excited through the $A\ ^2\Sigma^+$, $v'=0$ and 1 states. A model for TC-RFWM signals arising from transitions to quasibound resonances is applied to the observed line profiles of the $8p$ and $9p$, $v=1$ states. The decay rates extracted from the TC-RFWM spectra are compared to multichannel quantum defect theory (MQDT) calculations and multiphoton ionization (MPI) data. Transitions observed in the TC-RFWM spectra between the $A\ ^2\Sigma^+$, $v'=1$ state, downward in energy to the $v''=10$ vibrational level of the ground state are used to calibrate the intensity of the TC-RFWM spectra. From this calibration an excited-state cross section for the $9p$, $v=1$ state is derived.

II. TC-RFWM SPECTROSCOPY

TC-RFWM spectroscopy can, in many cases, be described conceptually in terms of light-induced gratings,[53] hence the name laser-induced grating spectroscopy (LIGS) and the labeling of the incident laser beams as grating and probe light in the four-wave mixing process. The technique is applied by crossing two laser beams at a small angle in a medium where they interfere to produce a sinusoidal modulation of light intensity. When the wavelength is tuned to a transition in the sample, the varying light intensity produces alternating regions of excited and ground-state populations. These alternating regions result in a Bragg diffraction grating characterized by a varying absorption coefficient and index of refraction. In this case, the grating is called a population grating because it arises from a population transfer due to excitation caused by the grating-forming laser beam. A signal is produced by scattering a third laser beam, the probe, off this grating to produce a fourth beam that propagates in a unique, well-defined direction. The four-wave mixing process is strongly enhanced when the frequency of the light

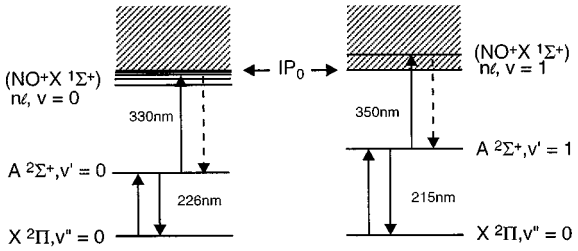

FIG. 1. Experimental arrangement for the TC-RFWM spectroscopy of NO.

corresponds to a molecular transition because of the resonant behavior of the third-order nonlinear susceptibility, $\chi(3)$, of the sample. A spectrum can be obtained by monitoring the intensity of the scattered signal beam as a function of the frequency of any of the input beams.

The TC-RFWM excitation schemes used in the experimental work presented here are shown in Fig. 1. Grating transitions are made between rovibrational levels of the $X\ ^2\Pi_{1/2}$ ground and $A\ ^2\Sigma^+$ excited electronic states of NO. Probe transitions are made between the $A\ ^2\Sigma^+$ state and the higher lying Rydberg states. Excited-state spectra are obtained by tuning the grating laser beam to a particular $A\ ^2\Sigma^+ \leftarrow X\ ^2\Pi_{1/2}$, rovibrational transition and scanning the probe beam frequency over $(NO^+X\ ^1\Sigma^+)nl \leftarrow A\ ^2\Sigma^+$ transitions while monitoring the intensity of the signal beam generated in the four-wave mixing process.

Diagrammatic perturbation theory provides a framework in which to calculate the $\chi(3)$ of the sample and thus the signal observed in RFWM spectroscopy.[53–57] For the experimental conditions and geometry of the work presented here, the TC-RFWM signal intensity as a function of the probe-laser frequency has been given by Williams and co-workers as[50]

$$S(\omega_p) \propto N^2 |\langle i|\mu|e\rangle|^4 |\langle e|\mu|f\rangle|^4 \mathfrak{T}(\omega_p) I_g^2 I_p, \tag{1}$$

where N is the number density of the medium, and I_g and I_p are the grating light and probe light intensities, respectively. Here we have assumed that the probe and grating light are linearly polarized, parallel to each other and that their bandwidths are negligible. The matrix element $|\langle i|\mu|e\rangle|$ represents the molecular dipole transition moment from the initial state to the intermediate excited state to which the grating light is tuned, and the matrix element $|\langle e|\mu|f\rangle|$ is the molecular dipole transition moment from the intermediate excited state to the final state across which the probe light is frequency tuned to obtain the TC-RFWM spectra. With the grating light on resonance, the line profile $\mathfrak{T}(\omega_p)$ as a function of the probe light frequency can be expressed as[51]

$$\mathfrak{T}(\omega_p) = \frac{1}{\Gamma_e^4} \times \frac{1}{(\omega_p - \omega_R)^2 + (\Gamma/2)^2}. \tag{2}$$

Equation (2) describes a Lorentzian profile as a function of the probe laser frequency ω_p with a full width at half-maximum (FWHM), Γ, and a peak resonance position at ω_R. Here, Γ_e is the decay rate of the intermediate excited state and Γ is the decay rate of the Rydberg state. Decay times are given by

$$\tau(\mathrm{s}) = \frac{1}{2\pi c \Gamma(\mathrm{cm}^{-1})}. \tag{3}$$

The signal expression in Eq. (1) applies to four-wave mixing schemes that access discrete states of a system. The analysis of the TC-RFWM signal when a state in the excitation scheme has a continuum character, such as the np Rydberg states probed in this study, requires a modified expression for the signal. A RFWM signal is calculated, in general, by summing over all of the states of the system in which the four-wave mixing is taking place. In practice, the application of the rotating-wave approximation (RWA) simplifies the calculation by determining a subset of resonant and nearly resonant terms that contribute significantly to the sum. When this procedure is carried out for the case of an isolated upper level resonance that consists of both a discrete and continuum character, the signal can be expressed as[52]

$$S(\omega_p) \propto N^2 |\langle i|\mu|e\rangle|^4 \times \left(\int_{D\eta} |\langle e|\mu|\eta\rangle|^2 L(\omega_p, \omega_g; \eta) d\eta \right)^2 I_g^2 I_p. \tag{4}$$

Here a configuration-interaction model[58] to describe the quasibound resonance in terms of a continuum states, $|c\rangle$, and discrete state, $|R\rangle$, coupled by an interaction Hamiltonian, V, has been used. The energy index,

$$\eta \equiv \frac{\omega_p - \omega_R}{\Gamma/2}, \tag{5}$$

where ω_R is the unperturbed resonance position of the discrete state, has been introduced to characterize the eigenstates, $|\eta\rangle$, of the coupled discrete and continuum state configurations. Here, $L(\omega_p, \omega_g; \eta)$ is a complex line shape factor. Applying the RWA in the analysis results in a range, D_η, of continuum states, $|\eta\rangle$, that must be included in the summation process.

In the configuration-interaction model, the transition probability for excitation of the eigenstate $|\eta\rangle$ is given by the well-known Beutler–Fano line profile,[58,59]

$$|\langle e|\mu|\eta\rangle|^2 = p_c \frac{(q+\eta)^2}{1+\eta^2} + p_u, \tag{6}$$

where p_c is the probability of exciting the continuum, $|\langle e|\mu|c\rangle|^2$, and p_u is the probability of making transitions to other uncoupled continua not interacting with the discrete state. The asymmetry parameter, q, is a measure of the relative strengths of the continuum and discrete dipole moments scaled by the interaction Hamiltonian, V. It is given by[58]

$$q \equiv \frac{\langle \eta|\mu|e\rangle}{\pi \langle R|V|c\rangle \langle c|\mu|e\rangle}, \tag{7}$$

with $\Gamma \propto |\langle R|V|c\rangle|^2$.

By substituting the transition probability given by Eq. (6) into the expression for the TC-RFWM signal in Eq. (4) and then integrating, assuming q, p_c, and p_u are energy independent near $\eta = 0$, the following expression for the TC-RFWM signal for probing a quasibound resonance is obtained:[52]

$$S(\omega_p) \propto N^2 |\langle i|\mu|e\rangle|^4 |\langle e|\mu|c\rangle|^4 \mathfrak{T}(\omega_p) I_g^2 I_p, \tag{8}$$

where the line shape function, $\mathfrak{T}(\omega_p)$, is given by

$$\mathfrak{T}(\omega_p) = \frac{1}{\Gamma_e^4} \left(\frac{(q^2+2r+1)^2 + \left(2q + (1+r) \frac{(\omega_p - \omega_R)}{\Gamma/2} \right)^2}{(\omega_p - \omega_R)^2 + 4(\Gamma/2)^2} \right), \tag{9}$$

with $r \equiv p_u/p_c$. The constants of proportionality omitted in Eqs. (1) and (8) are the same in both cases. By fitting the appropriate lineshape functions to observed TC-RFWM profiles, valuable dynamical information in the form of the r, q, and Γ parameters can be determined.

III. EXPERIMENT

A. Spectroscopic background

The levels accessed in the excitation scheme shown in Fig. 1 are denoted as follows:

$$A\ ^2\Sigma^+, v', N^+{}', N', J' \leftarrow X\ ^2\Pi_{1/2}, v''=0, J'', \tag{10}$$

$$(NO^+ X\ ^1\Sigma^+) nl, v, N^+, N, J \leftarrow A\ ^2\Sigma^+, v', N^+{}', N', J'. \tag{11}$$

Throughout the discussion, levels of the $X\ ^2\Pi_{1/2}$ state are denoted with double primes, levels of the $A\ ^2\Sigma^+$ state are denoted with single primes, and Rydberg levels of $v=0$ and 1 are denoted without primes. For low rotational levels, the $X\ ^2\Pi_{1/2,3/2}$ states are best described by using Hund's case (a) coupling. The F_1 component with $\Omega'' = \frac{1}{2}$ is well separated from the F_2 component with $\Omega'' = \frac{3}{2}$, which lies 124.9 cm^{-1} higher in energy.[60] The $A\ ^2\Sigma^+$ state is close to Hund's case (b) coupling and is described by the total angular momentum, J', the total angular momentum exclusive of spin, N', and the rotational angular momentum of the NO^+ ion core, $N^+{}'$. Although N^+ is not generally a good quantum number in Hund's case (b) coupling, $N' = N^+{}'$ for the $A\ ^2\Sigma^+$ state because the excited electron is in the $3s\sigma$ orbital. The levels are labeled F_1 for $J' = N' + \frac{1}{2}$ and F_2 for $J' = N' - \frac{1}{2}$, where $\frac{1}{2}$ is total electronic spin of the molecule. The grating-forming transitions in Eq. (10) are denoted in the standard way, for example, $R_{21}(J'')$ indicates a transition from the $X\ ^2\Pi_{1/2}$ (the F_1 component) state to the F_2 component of the $A\ ^2\Sigma^+$ state, and $J' = J'' + 1$. The splitting between the different J' levels with the same value of N' is not resolved in the present study. Because the O_{21} branch, however, is not allowed in single-photon excitation for parity reasons, the P_{11} branch is not overlapped and it can be used to selectively excite a pure F_1 spin state, i.e., a single J' level, for a series of N' levels.

High Rydberg states are generally described by using Hund's case (d) coupling in which, l, the angular momentum of the Rydberg electron, is uncoupled from the nuclear axis and N^+, the rotational angular momentum of the NO^+ ion core, and N, the total angular momentum exclusive of spin, are good quantum numbers. The projection of l on the internuclear axis is denoted $\mathscr{L}$ and the total angular momentum, N, takes on the values $N = N^+ + \mathscr{L}$. The F components

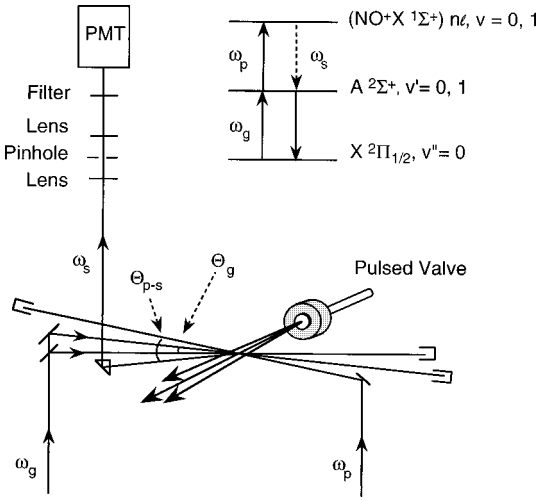

FIG. 2. The TC-RFWM schemes used to probe the $(NO^+X\ ^1\Sigma^+)nl$, $v=0$ and 1 Rydberg states of NO.

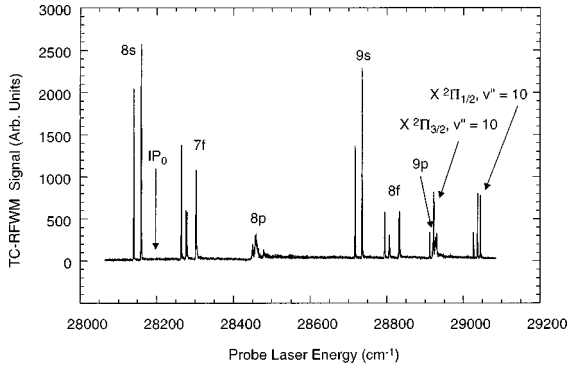

FIG. 3. The TC-RFWM spectrum obtained by tuning the grating-forming lasers to the $R_{11}(1.5)$ branch of the $A\ ^2\Sigma^+,\ v'=1 \leftarrow X\ ^2\Pi_{1/2},\ v''=0$ transition and scanning the probe laser in the energy region of transitions to several $(NO^+X\ ^1\Sigma^+)nl,\ v=1$ Rydberg states lying at and just above the $v=0$ ionization potential.

are defined in the same way as described above (F_1 for $J=N+\frac{1}{2}$ and F_2 for $J=N-\frac{1}{2}$). Because the F components are not resolved in the present study, the probe transitions in Eq. (11) are denoted in terms of N as $^{N'-N^+}\Delta N_{\mathscr{L}}$.

Because the electron is decoupled from the molecular axis in both the $A\ ^2\Sigma^+$ state and the high Rydberg states, transitions between different F components are weak. Thus, $F_1 \leftarrow F_1'$ transitions are expected to be much stronger than $F_2 \leftarrow F_1'$ transitions. Similarly, because the coupling between l of the Rydberg electron and the rotation of the nuclei is small in both the $A\ ^2\Sigma^+$ state, which has $l=0$, and the high Rydberg states, transitions with $N^+-N'=N^+-N^{+\prime}=0$ are expected to be strongest.

The orbital of the excited electron in the $A\ ^2\Sigma^+$ state is predominantly $3s$ with small amounts of d and p character mixed in.[61] This suggests that while transitions to the np Rydberg states will be strongest, transitions to ns, nd, and nf Rydberg states are also allowed. The allowed single-photon transitions from the $A\ ^2\Sigma^+$ state to the high Rydberg states are restricted by the selection rules $\Delta J=0, \pm 1$ and an odd parity change. This results in the following derived selection rule for the observed transitions: for even-l Rydberg states, N^+-N' must be odd and cannot be equal to zero; for odd-l Rydberg states, N^+-N' must be even and therefore can take on the value of zero.[24]

B. Experimental arrangement

Figure 2 shows a schematic diagram of the experimental arrangement. Light pulses at 226 and 215 nm, used to excited the $v'=0$ and $v'=1$ levels of the $A\ ^2\Sigma^+$ state, respectively, are generated by frequency doubling the output of a pulsed Nd:YAG-pumped dye laser. Light pulses at 350 and 330 nm; used to excite the $n=7-9$, $v=1$ Rydberg states and the $n=16-30$, $v=0$ Rydberg states, respectively, were produced by a second pulsed Nd:YAG-pumped dye laser. All laser beams were collimated to a diameter of ~ 2 mm and were linearly polarized parallel to one another. Laser pulse energies could be varied from 10 to 300 μJ per pulse. Light pulses from the two lasers were ~ 8 ns in duration and data were taken with a delay of ~ 20 ns between the grating-forming pulses and the probe pulses. The bandwidth of the probe laser light was 0.4 cm^{-1}. The wavelength of the probe laser light was calibrated by recording the optogalvanic spectra of sodium and argon simultaneously with the LIGS spectrum.[62]

A molecular beam was produced by a pulsed valve operated with a backing pressure of ~ 1 atm of pure NO. The major velocity component of the molecular beam was arranged to be parallel to the grating fringes to minimize the decay of the grating due to molecular motion. With this arrangement the grating persisted for ~ 100 ns. Grating light, with frequency $\omega_g=2\pi c/\lambda_g$, was divided into two beams that were crossed at a small angle, $\Theta_g=3°$, in the interaction region to form the grating. Probe light, ω_p, was then scattered off the grating to produce the signal beam, ω_s. The angle of incidence for the probe beam is restricted by the phase-matching constraint, equivalent to the Bragg scattering condition $\lambda_g/\sin(\Theta_g/2)=\lambda_p/\sin(\Theta_{p\text{-}s}/2)$.[53] The signal beam was detected through a spatial filter consisting of a telescope and pinhole. A color filter was used to further reduce background due to scattered light.

IV. RESULTS AND DISCUSSION

A. $v=1$ Rydberg states

Figure 3 shows an example of a TC-RFWM spectra as a function of the probe laser frequency in the energy region from $\sim 28\,100$ cm^{-1} to $\sim 29\,100$ cm^{-1}, which includes energies at and above the $v=0$ ionization potential of NO. Transitions from the $A\ ^2\Sigma^+$, $v'=1$, $N'=2$ level to several members of the nl, $v=1$ Rydberg series are identified. TC-RFWM spectra were recorded for the $P_{11}(1.5)$, $P_{11}(2.5)$, $R_{11}(0.5)$, $R_{11}(1.5)$, $R_{11}(2.5)$, and $R_{11}(3.5)$ branches of the $A\ ^2\Sigma^+,\ v'=1 \leftarrow X\ ^2\Pi_{1/2},\ v''=0$ grating transition. For each Rydberg state, the probe transition energies observed in the TC-RFWM spectra agree with previously reported values to within the energy uncertainty of 0.5 cm^{-1}. These include measured energies for the $8s$ and $9s$, $v=1$ Rydberg states,[2,4,14,19] the $7f$[2,14,18,21] and $8f$,[2] $v=1$ Rydberg states, and the $8p$[14] and $9p$,[2,4] $v=1$ states. Also visible in the TC-

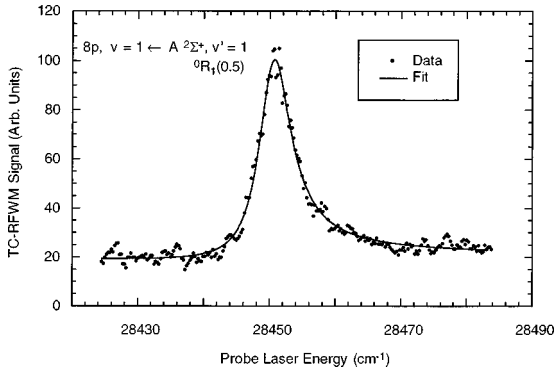

FIG. 4. The $8p$, $v=1$, $N^+=1$, $N=1$, $J=1.5$ resonance observed by TC-RFWM via the $P_{11}(1.5)$ branch of the $A\ ^2\Sigma^+$, $v'=1 \leftarrow X\ ^2\Pi_{1/2}$, $v''=0$ grating transition and the $^0R_1(0.5)$ branch of the $(NO^+X\ ^1\Sigma^+)8p$, $v=0 \leftarrow A\ ^2\Sigma^+$, $v'=1$ probe transition. The solid line is a least-squares fit of the data to the TC-RFWM line profile given in Eq. (9).

RFWM spectra are additional transitions close in energy to the $9p$, $v=1$ states. These peaks arise from transitions downward in energy to the $v''=10$ level of the $X\ ^2\Pi_{1/2,3/2}$ ground state in the four-wave mixing process.

The Rydberg states of NO probed in this study lie above the $N(^2D)+O(^3P)$ and the $N(^4S)+O(^3P)$ dissociation limits to which several doublet valence states converge. Calculations[29–35] and experimental studies[7–9,11,20–22,27] have shown that the interactions of Rydberg states with valence states lead to dissociation at varying rates that can change depending on the angular momentum and rotational quantum numbers of the Rydberg state. In the particular case of the np Rydberg series, photofragment studies[20,22] provide strong evidence that the np states observed in the present study decay primarily by dissociation through interaction with the continuum of the $B\ ^2\Pi$ valence state, which converges to the $N(^2D)+O(^3P)$ limit. Even above the ionization limit where autoionization decay processes are energetically possible and do compete with dissociation, the experimental evidence[20] indicates that the $8p$ and $9p$, $v=1$ states decay predominantly through this dissociation channel.

A measurement of the decay rate of the $8p$ and $9p$, $v=1$ Rydberg states can be made by fitting the function in Eq. (9), appropriate for the excitation of a quasibound resonance in the RFWM process, to the line profile observed in the TC-RFWM spectra. For the $8p$ and $9p$, $v=1$ states, p_c is interpreted as the probability of transition to the dominant $B\ ^2\Pi$ valence state coupled to the $8p$ and $9p$, $v=1$ Rydberg states, Γ is the predissociative decay rate of the Rydberg state, q is the asymmetry parameter characterizing the relative strengths of the transition moments to the Rydberg state and the dissociative continuum, and p_u is the transition probability to any noninteracting continua.

Figure 4 shows a fit of the TC-RFWM line profile in Eq. (9) to the measured profile of the $^0R_1(0.5)$ branch of the probe transition to the $N=1$, $J=1.5$ level of the $8p$, $v=1$ Rydberg state. In this case, the $J'=0.5$ level of the $A\ ^2\Sigma^+$ was selectively excited by the $P_{11}(1.5)$ branch of the grating transition and thus a single J level of the Rydberg state is accessed in the probe transition. Table I summarizes the fit results for this transition. The q and r parameter values are very sensitive to the background level of the signal and care was taken to establish the zero for the observed signal by blocking each input laser beam to distinguish between the contributions of any scattered light getting into the detector and the true signal beam. The statistical uncertainties associated with the fit parameters indicate that the line profile in Eq. (9) does very well in characterizing all aspects of the observed profile, including the asymmetry of the feature and the observed background level.

TABLE I. Fit results for the $8p$ and $9p$, $v=1$, $N^+=1$, $N=1$, $J=1.5$ Rydberg states of NO. The first uncertainty listed is the standard deviation from multiple measurements of the line profiles; the second is the average statistical uncertainty obtained in the fits.

	$8p$	$9p$
Energy (cm^{-1})	28 450.7 (0.4) (0.05)	28 922.3 (0.5) (0.07)
Γ (cm^{-1})	2.85 (0.16) (0.06)	1.41 (0.25) (0.08)
q	4.6 (0.7) (0.2)	4.2 (0.2) (0.3)
r	9.5 (1.6) (0.9)	21.3 (2.2) (3.2)
C^2		831 (37) (20)

In Table II, the fit results for the decay rate, Γ, are compared to MPI[13] measurements and MQDT calculations[33] of Γ for the $8p$ and $9p$, $v=1$ states. The procedure for fitting the $9p$, $v=1$ data is discussed below. While a comparatively smaller width for the $9p$ state is observed in both the MPI and the TC-RFWM data, the absolute values measured with each technique, especially for the $9p$ state, are in disagreement. A comparison of the measured TC-RFWM decay rate to the MQDT decay rate requires some discussion. The TC-RFWM widths presented here were extracted from the data by assuming a configuration interaction of the Rydberg states with a single continuum channel. In comparison, the MQDT treatment is more complete and includes several ionization channels and two dissociation channels.[32,33] As discussed above, however, the decay of the $8p$ and $9p$ states proceeds by dissociation through a single dominant channel,[20] and thus the simpler model is justified and the results obtained with it can be compared to the fuller treatment. To the extent that this is a valid approach, the good agreement observed between the decay rates obtained by using TC-RFWM and those calculated by MQDT, especially in the case of the $9p$, $v=1$ state, is meaningful.

Because the $8p$ and the $9p$ states belong to the same Rydberg-state channel and both lie in the continuum energy region of the $B\ ^2\Pi$ valence state, one might expect the q and r parameters to be similar for the $8p$ and $9p$ states, and the decay rates, Γ, to scale as $1/n^3$. Not all of these behaviors, however, is observed. In the configuration interaction be-

TABLE II. A comparison of measured and calculated values of Γ (cm^{-1}) for the $8p$ and $9p$, $v=1$ resonances.

	TC-RFWM	MPI[a]	Calculated Γ (cm^{-1})[b]
$8p$	2.85	3.9	4.9
$9p$	1.41	3.0	1.8

[a]Multiphoton ionization spectra; Ref. 13.
[b]MQDT calculation; Ref. 33.

tween the Rydberg state and the continuum of the $B\ ^2\Pi$ valence state, the intersection of the potential energy curve of the $8p$ and the $9p$ Rydberg states with the inner part of the $B\ ^2\Pi$ potential energy curve will occur at different internuclear separations that would change the overlap of the two wave functions and could measurably affect the size of the configuration interaction as a function of energy. The slightly smaller decay rate observed for the $9p$ state indicates a smaller configuration interaction with the $B\ ^2\Pi$ state continuum in comparison to the $8p$ state, which could be indicative of such an effect.

The r parameter can be interpreted in two ways. Making, first, the assumption that the transition moment to the noninteracting continuum does not vary over the energy difference between the $9p$ and $8p$ states, the larger r value for the $9p$ state, compared to the $8p$ state, implies a smaller transition moment to the interacting continuum at the energy of the $9p$ state. As described by Eq. (7), a smaller interaction Hamiltonian and a smaller value for p_c would suggest a larger value of q for the $9p$ state. Somewhat surprisingly, however, a nearly equal value of q is observed for the $9p$ state. This result implies a transition moment for the excitation of the perturbed $8p$ state that is ~ 2.3 times larger than the transition moment to the perturbed $9p$ state. This value is almost twice as large as the factor of 1.2 obtained by scaling the transition moments by $n^{-3/2}$. Making, instead, the assumption that the difference in the r parameter for the $8p$ and the $9p$ state energies is due mainly to a variation with energy of uncoupled continua, the difference in q values for the $8p$ and $9p$ lineshapes implies a transition moment for the excitation of the perturbed $8p$ state that is only ~ 1.5 times larger than the transition moment to the perturbed $9p$ state. In either case, however, the differences in the parameters observed for the $8p$ and $9p$ states that are not accounted for by n-scaling factors are evidence for a significant variation in the structure of the continua over an energy range equal to the energy difference ($\sim 450\ \mathrm{cm}^{-1}$) between the $8p$ and $9p$ states.

B. Excited-state absorption cross section of the $9p$, $v=1$ Rydberg state

In Fig. 3 unexpected transitions are visible in the TC-RFWM spectrum close in energy to peaks corresponding to transitions to the $9p$, $v=1$ Rydberg state. The source of these resonances was determined to be $X\ ^2\Pi_{3/2,1/2}$, $v''=10$, $J''\leftarrow A\ ^2\Sigma^+$, v', N', J' probe transitions downward in energy in the four-wave mixing process. This explanation is supported by the absence of these transitions in a double-resonance MPI spectrum taken over the same energy region[63] and was further confirmed by a comparison of the observed peak energies to transition energies calculated with measured spectroscopic constants for the $X\ ^2\Pi_{3/2,1/2}$, $v''=10$ level of the ground state.[64] Because the absolute oscillator strengths and Einstein coefficients of the $A\ ^2\Sigma^+$, $v'\leftarrow X\ ^2\Pi_{1/2,3/2}$, v'' transitions of NO are well established,[65,66] these transitions can be used to calibrate the magnitude of the TC-RFWM spectrum and derive a value for the $A\ ^2\Sigma^+$-state photoabsorption cross section of the $9p$, $v=1$ Rydberg state.

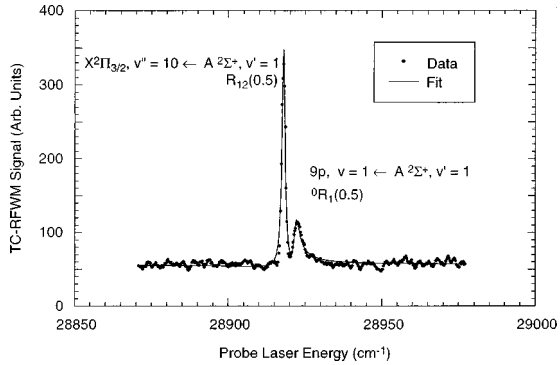

FIG. 5. The $9p$, $v=1$, $N^+=1$, $N=1$, $J=1.5$ and the $X\ ^2\Pi_{3/2}$, $v''=10$, $J''=1.5$ resonances observed by TC-RFWM via the $P_{11}(1.5)$ branch of the $A\ ^2\Sigma^+$, $v'=1\leftarrow X\ ^2\Pi_{1/2}$, $v''=0$ grating transition and the ${}^0R_1(0.5)$ branch of the $(\mathrm{NO}^+X\ ^1\Sigma^+)9p$, $v=0\leftarrow A\ ^2\Sigma^+$, $v'=1$ probe transition and the $R_{12}(0.5)$ branch of $X\ ^2\Pi_{3/2}$, $v''=10\leftarrow A\ ^2\Sigma^+$, $v'=1$ probe transition, respectively.

Neglecting any possible coherent addition of the $\chi(3)$ amplitudes, the sum consisting of the line shapes given by Eqs. (2) and (9),

$$S(\omega_p)\propto \frac{C^2}{(\omega_p-\omega_X)^2+(\Gamma_X/2)^2} + \frac{(q^2+2r+1)^2+\left[2q+(1+r)\dfrac{\omega_p-\omega_R}{(\Gamma_R/2)}\right]^2}{(\omega_p-\omega_R)^2+4(\Gamma_R/2)^2}, \tag{12}$$

can be fitted to the adjacent $X\ ^2\Pi_{3/2}$, $v''=10$ and $9p$, $v=1$ peaks observed in the TC-RFWM spectrum. Here, Γ_X is the FWHM and ω_X is the resonance position of the $X\ ^2\Pi_{3/2}$, $v''=10\leftarrow A\ ^2\Sigma^+$, $v'=1$ transition profile. Similarly, Γ_R is the FWHM and ω_R is the resonance position of the $9p$, $v=1\leftarrow A\ ^2\Sigma^+$, $v'=1$ transition profile. Comparing Eqs. (1) and (8), the constant C^2 is defined as the ratio of the squared transition probabilities,

$$C^2=\frac{|\langle e|\mu|f\rangle|^4}{|\langle e|\mu|c\rangle|^4}=\frac{\mu_{ef}^4}{p_c^2}. \tag{13}$$

Because in both transitions the same J is accessed, specific expressions for the rotational line strengths in each case are not required in this analysis.

The results of the fit of Eq. (12) to the $X\ ^2\Pi_{1/2}$, $v''=10\leftarrow A\ ^2\Sigma^+$, $v'=1$ and the $9p$ $v=1\leftarrow A\ ^2\Sigma^+$, $v'=1$ transitions are shown in Fig. 5 and values for the fitted parameters are given in Table II. To obtain these results, Γ_X was set equal to the bandwidth of the probe laser since the linewidth that would result from the natural rate of decay of this state is much less than the laser bandwidth. The energy of the transition to the $J''=1.5$ level of the $X\ ^2\Pi_{1/2}$, $v''=10$ state was determined in the fit to be $28\,918.1\ \mathrm{cm}^{-1}$, in good agreement with previous measurements of $X\ ^2\Pi_{1/2}$, $v''=10$ state energies.[64]

From the fit results the cross section for photoabsorption of the $9p$, $v=1$ state from the $A\ ^2\Sigma^+$, $v'=1$ state can be calculated. The cross section can be expressed in terms of the continuum states as[65]

$$\sigma(\omega_p)=\frac{\pi\omega_p}{3\hbar c\epsilon_0}|\langle e|\mu|\eta\rangle|^2. \tag{14}$$

Substituting Eq. (6) into this expression, the cross section is expressed in terms of the fit parameters as

$$\sigma(\omega_p)=\frac{\pi}{3\hbar c\epsilon_0}\frac{\nu(\mathrm{cm}^{-1})}{\Gamma(\mathrm{cm}^{-1})}\frac{|\mu_{fe}|^2}{C}\left(\frac{(q+\eta)^2}{1+\eta^2}+r\right). \tag{15}$$

The factor of Γ in Eq. (15) comes from the energy normalization of the continuum states.

From the experimentally determined Einstein coefficient, $A_{1,10}=2.944\times10^4\ \mathrm{s}^{-1}$,[66] for the $X\ ^2\Pi_{3/2},\ v''=10 \leftarrow A\ ^2\Sigma^+,\ v'=1$ transition, a value of $|\langle e|\mu|f\rangle|^2=4.3\times10^{-62}\ \mathrm{C}^2\ \mathrm{m}^2$ for the transition moment is calculated. Substituting in the values for C, v, and Γ listed in Table II and the dipole transition moment for the $X\ ^2\Pi_{3/2},\ v''=10 \leftarrow A\ ^2\Sigma^+,\ v'=1$ transition, we obtain the following expression for the photoabsorption cross section for the $9p,\ v=1$ Rydberg state:

$$\sigma(\omega_p)=1.2\times10^{-22}m^2\left(\frac{(q+\eta)^2}{1+\eta^2}+r\right). \tag{16}$$

The uncertainty of the excited-state cross section is estimated to be $\sim25\%$, based on variations observed in the C^2 parameter determined from several wavelength scans. The maximum in the cross section occurs at an energy $\omega_p=\omega_{\max}$, when $\eta=1/q$, which is slightly shifted from the actual resonance position, ω_R, of the Rydberg state. At $\omega_{\max}$, the term $(q+\eta)^2/(1+\eta^2)$ becomes q^2+1. Evaluating Eq. (16) at its maximum using the q and r values given in Table II, the maximum in the cross section is found to be $46.3\times10^{-22}\ \mathrm{m}^{-2}$ or 46.3 Mb. This maximum value is comparable to the value of 22.1 Mb for the maximum in the ground-state photoabsorption cross section of the $9p,\ v=1$ state calculated with a MQDT treatment by Giusti-Suzor and Jungen.[32] It is somewhat larger, however, than the value of 2.7 Mb obtained for the $9p,\ v=1$ state by scaling by n^{-3} the cross section value of 0.94 Mb for the $13p,\ v=1$ state measured by using fluorescence depletion in the $A\ ^2\Sigma^+$ state.[13]

The uncertainties given in Tables I and II only include the statistical uncertainties of the fits and the standard deviation of multiple measurements. Other sources of experimental uncertainty include possible power broadening of the transitions and the effect of the finite bandwidth of the probe laser on the line profiles. Probe laser power studies were conducted to examine the behavior of the linewidths as a function of the power of the probe laser pulses. For probe-pulse energies below 100 μJ, the fitted linewidths did not measurably change. Above 100 μJ, the widths began to increase with increasing laser power. The magnitude of the TC-RFWM signal was also examined as a function of the probe laser power. As expected from Eqs. (1) and (4), the TC-RFWM signal varied linearly with the energy of the probe pulses for values below 150 μJ. At pulse energies greater than 150 μJ, the signal intensity began to saturate. As a consequence of this observed trend with laser power, the parameter results presented here are based on data taken with probe-pulse energies below 100 μJ.

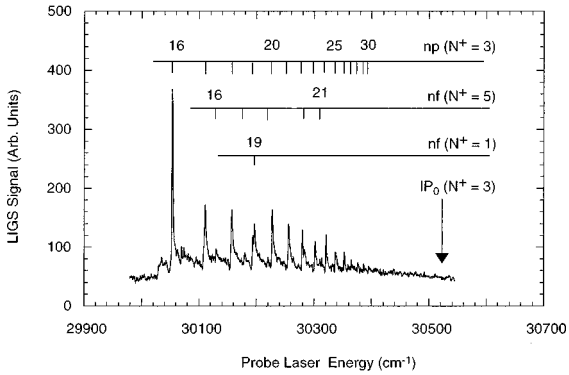

FIG. 6. The TC-RFWM spectrum obtained by tuning the grating forming laser to the $R_{11}(2.5)$ branch of the $A\ ^2\Sigma^+,\ v'=1 \leftarrow X\ ^2\Pi_{1/2},\ v''=0$ transition and scanning the probe laser in the energy region of transitions to numerous $(\mathrm{NO}^+X\ ^1\Sigma^+)nl,\ v=0$ Rydberg states lying below the $v=0$ ionization potential.

The laser bandwidth of the 350 nm probe radiation is $\sim0.4\ \mathrm{cm}^{-1}$. An estimate of the effect of this finite bandwidth on the extracted widths of the predissociating Rydberg states was assessed by doing a numerical convolution of a Gaussian curve with a FWHM of $0.4\ \mathrm{cm}^{-1}$ with the TC-RFWM line profile given in Eq. (9), incorporating the parameters observed for the ${}^0R_1(0.5)$ branch of the probe transition to the $8p,\ v=1$ state. The effect on the apparent width of the profile was less than $\sim5\%$ for this case. An analytic expression for the TC-RFWM line profile that includes finite laser bandwidth effects would be useful and is currently being investigated.

C. $v=0$ Rydberg states

Figure 6 shows the TC-RFWM spectrum observed via the $R_{11}(2.5)$ branch of the $A\ ^2\Sigma^+,\ v'=1 \leftarrow X\ ^2\Pi_{1/2},\ v''=0$ grating transition as a function of the probe laser frequency in the energy region from 30 000 cm^{-1} to the ionization potential near 30 550 cm^{-1}. Transitions from the $A\ ^2\Sigma^+,\ v'=0,\ J'=3.5,\ N'=3$ level to members of the np and nf Rydberg series are observed, and their term energies and quantum defects are reported in Table III. The strong transitions observed in this spectra are identified as belonging to the np series converging to the $v^+=0,\ N^+=3$ level of the ground state of the NO^+ ion. The weaker series consist of transitions to levels of the nf states converging principally to the $N^+=5$ level of the ion core. These Rydberg series can be analyzed with the well-known Rydberg formula,

$$E=\mathrm{IP}_{v^+,N^+}-\frac{\mathrm{Ry}}{(n-\delta)^2}. \tag{17}$$

The best fit of Eq. (17) to the observed energies of the $np,\ v=0$ series is obtained with a quantum defect of 0.71 ± 0.01 and an ionization potential of $74745.9\pm0.4\ \mathrm{cm}^{-1}$ for the $v^+=0,\ N^+=3$ level of the ion core. By using the rotational constant for the ground vibrational state of the ion, $B=1.997\ \mathrm{cm}^{-1}$,[60] the ionization potential for the rotationless core is found to be $\mathrm{IP}_{0,0}=74721.9\pm0.4\ \mathrm{cm}^{-1}$, which is in good agreement with the value of $74\,721.67\pm0.10\ \mathrm{cm}^{-1}$ measured by Biernacki *et al.*[18] A fit of Eq. (17) to the ob-

TABLE III. Term energies, quantum defects, and assignments of the $(NO^+X\ ^1\Sigma^+)np$ and nf, $v=0$ Rydberg states observed by TC-RFWM via the $J'=3.5$, $N'=3$ level of the $A\ ^2\Sigma^+$, $v'=0$ state (44 222.77 cm^{-1}). The uncertainty in the energies is $\pm 0.5\ cm^{-1}$.

nl	Energy (cm^{-1})	$\delta(N^+=1)$	$\delta(N^+=3)$	$\delta(N^+=5)$
16*p*	74 276.4		0.71	
17*p*	74 333.2		0.69	
16*f*	74 352.6			0.01
18*p*	74 379.6		0.69	
17*f*	74 402.4			−0.01
19*p*	74 416.6		0.74	
19*f*	74 419.1	0.08		
18*f*	74 443.1			0.00
20*p*	74 450.3		0.73	
21*p*	74 478.7		0.72	
22*p*	74 502.2		0.77	
20*f*	74 505.8			0.05
23*p*	74 524.4		0.73	
21*f*	74 532.9			−0.01
24*p*	74 543.5		0.70	
25*p*	74 560.4		0.66	
26*p*	74 575.2		0.62	
27*p*	74 587.2		0.68	
28*p*	74 599.1		0.63	
29*p*	74 609.2		0.64	
30*p*	74 617.9		0.69	

served energies of the nf series converging to the $v^+=0$, $N^+=5$ level of the ion core yields a quantum defect of $\delta=0.00\pm0.04$ and an $IP_{0,0}=74721.4\pm0.4\ cm^{-1}$, also in good agreement with previous measurements and the result from the analysis of the np series.

The background level above zero in Fig. 6 is a real FWM signal that indicates the contribution of a continuum to the signal. This energy region includes the continua of the $B\ ^2\Pi$, $L\ ^2\Pi$, $B'\ ^2\Delta$, and $I\ ^2\Sigma^+$ states, which converge to the $N(^2D)+O(^3P)$ dissociation limit, and the $A'\ ^2\Sigma$ state, which converges to the $N(^4S)+O(^3P)$ dissociation limit, thus several states could be contributing to the observed continuum signal in this region.

For intermediate and higher values of principal quantum number, the $v=0$ Rydberg states of NO have been difficult to observe in the past because of their low ionization efficiency and significant rates of predissociation. As noted recently by Geng *et al.*,[46] who have made similar measurements to those reported here in an energy range that includes several $n=7-13$, $v=0$ Rydberg states, these results demonstrate that TC-RFWM can provide a useful alternative technique that in some circumstances may be better suited than photoionization to detect rapidly decaying states with competing ionization and dissociation decay processes. In the energy region probed by this study, Ebata *et al.*[5,6] used two-color multiphoton ionization through the $A\ ^2\Sigma^+$ state to excite high-lying, $v=0$, np Rydberg states of NO in a room temperature cell. The Rydberg states were then detected by collisional ionization. They reported energies for np states from $n=15-30$ converging to the $N^+=0$ level of the ion. The energies reported here for the np series converging to the $N^+=3$ level of NO^+ in Table III are consistent with these previous measurements. To our knowledge, energies for the $n=16-21$ members of the $v=0$, nf Rydberg states have not been reported before.

V. CONCLUSIONS

Nonlinear optical techniques continue to be developed and applied as distinct and useful probes in gas-phase molecular spectroscopy. The absorption-like nature of the TC-RFWM signal makes it a particularly favorable approach for the study of excited states that rapidly convert their energy and therefore are difficult to observe with fluorescence or ionization techniques. Here, Rydberg states of NO both above and below the first ionization potential have been observed by using TC-RFWM spectroscopy. The observation of the $v=0$ Rydberg states by using the zero-background TC-RFWM technique in field-free conditions illustrates the advantages this technique can offer.

The possibility of doing quantitative dynamical studies on highly excited and rapidly decaying molecular Rydberg states by using TC-RFWM techniques has also been demonstrated. Decay times of the quasibound $8p$ and $9p$, $v=1$ Rydberg states have been extracted from the observed spectra by using a recently developed theoretical model for the TC-RFWM signal intensities and line profiles of quasibound states whose decay dynamics are well described by a configuration-interaction treatment. The decay rates have been compared to those computed from MQDT calculations and observed previously in MPI measurements. In addition, transitions observed in the TC-RFWM spectra from the $A\ ^2\Sigma^+$, $v'=1$ state downward in energy to the $v''=10$ vibrational level of the $X\ ^2\Pi_{3/2}$ ground state have been used to derive a cross section of 46.3 Mb for absorption from the $A\ ^2\Sigma^+$, $v'=1$ state to the $9p$, $v=1$ Rydberg state.

ACKNOWLEDGMENTS

This work was supported by the National Science Foundation, Grant No. PHY-9623569 and by the U.S. Department of Energy, Office of Energy Research, Office of Basic Energy Sciences, under Contract No. W-31-109-Eng-38.

[1] C. H. Greene and Ch. Jungen, Adv. At. Mol. Phys. **21**, 51 (1985).
[2] E. Miescher, Can. J. Phys. **54**, 2074 (1976).
[3] E. Miescher and F. Alberti, J. Phys. Chem. Ref. Data **5**, 309 (1976).
[4] E. Miescher and K. P. Huber, in *International Review of Science* (Butterworths, London, 1976), Vol. 2, p. 37.
[5] T. Ebata, Y. Anazaki, M. Fujii, N. Mikami, and M. Ito, J. Phys. Chem. **87**, 4773 (1983).
[6] T. Ebata, N. Mikami, and M. Ito, J. Chem. Phys. **78**, 1132 (1983).
[7] M. Seaver, W. A. Chupka, S. D. Colson, and D. Gauyacq, J. Phys. Chem. **87**, 2226 (1983).
[8] S. Fredin, D. Gauyacq, M. Horani, Ch. Jungen, G. Lefevre, and F. Masnou-Seeuws, Mol. Phys. **60**, 825 (1987).
[9] W. Y. Cheung, W. A. Chupka, S. D. Colson, D. Gauyacq, P. Avouris, and J. J. Wynne, J. Chem. Phys. **78**, 3625 (1983).
[10] W. Y. Cheung, W. A. Chupka, S. D. Colson, D. Gauyacq, P. Avouris, and J. J. Wynne, J. Phys. Chem. **90**, 1086 (1986).
[11] Y. Achiba, K. Sato, and M. K. Kimura, J. Chem. Phys. **82**, 3959 (1985).
[12] S. T. Pratt, Chem. Phys. Lett. **151**, 138 (1988).
[13] Y. Anazaki, T. Ebata, N. Mikami, and M. Ito, Chem. Phys. **89**, 103 (1984).
[14] Y. Anezaki, T. Ebata, N. Mikami, and M. Ito, Chem. Phys. **97**, 153 (1985).
[15] J. W. J. Verschuur, J. Kimman, H. B. van Linden van den Heuvell, and M. van der Wiel, Chem. Phys. **103**, 359 (1986).

[16] E. E. Eyler and D. T. Biernacki, J. Chem. Phys. **88**, 2859 (1988).
[17] D. T. Biernacki, S. D. Colson, and E. E. Eyler, J. Chem. Phys. **88**, 2099 (1988).
[18] D. T. Biernacki, S. D. Colson, and E. E. Eyler, J. Chem. Phys. **89**, 2599 (1988).
[19] A. Nussenzweig and E. E. Eyler, J. Chem. Phys. **101**, 4617 (1994).
[20] A. Fujii and N. Morita, Chem. Phys. Lett. **182**, 304 (1991).
[21] A. Fujii and N. Morita, J. Chem. Phys. **97**, 327 (1992).
[22] A. Fujii and N. Morita, J. Chem. Phys. **98**, 4581 (1993).
[23] G. E. Gadd, L. E. Jusinski, and J. G. Slanger, J. Chem. Phys. **91**, 3378 (1989).
[24] S. T. Pratt, J. L. Dehmer, and P. M. Dehmer, J. Chem. Phys. **90**, 2201 (1989).
[25] S. T. Pratt, Ch. Jungen, and E. Miescher, J. Chem. Phys. **90**, 5971 (1989).
[26] H. Park and R. N. Zare, J. Chem. Phys. **106**, 2239 (1997).
[27] S. T. Pratt, J. Chem. Phys. **108**, 7131 (1998).
[28] For a review of photoionization dynamics see S. T. Pratt, Rep. Prog. Phys. **58**, 821 (1995).
[29] R. Gallusser and K. Dressler, J. Chem. Phys. **76**, 4311 (1982).
[30] R. deVivie and S. D. Peyerimhoff, J. Chem. Phys. **89**, 3028 (1988).
[31] H. Sun and H. Nakmura, J. Chem. Phys. **93**, 6491 (1990).
[32] A. Giusti-Suzor and Ch. Jungen, J. Chem. Phys. **80**, 986 (1984).
[33] M. Raoult, J. Chem. Phys. **87**, 4736 (1987).
[34] M. K. Nakashima, H. Nakamura, Y. Achiba, and K. Kimura, J. Chem. Phys. **91**, 1603 (1989).
[35] J. Guo, A. Mank, and J. W. Hepburn, Phys. Rev. Lett. **74**, 3584 (1995).
[36] The following are review articles discussing applications of RFWM spectroscopy in the gas phase: J. T. Fourkas and M. D. Fayer, Acc. Chem. Res. **25**, 227 (1992); R. L. Farrow and D. J. Rakestraw, Science **257**, 1894 (1992); G. Hall and J. Whitaker, J. Chem. Soc., Faraday Trans. **90**, 1 (1994).
[37] P. H. Vaccaro, in *Molecular Dynamics and Spectroscopy by Stimulated Emission Pumping*, edited by H. L. Dai and R. W. Field, Advances in Physical Chemistry Series, edited by C.-Y. Ng (World Scientific, Singapore, 1995), Vol. 4, p. 1.
[38] T. Muller and P. H. Vaccaro, Chem. Phys. Lett. **266**, 575 (1997).
[39] B. Hemmerling, R. Bombach, and W. Hubschmid, Chem. Phys. Lett. **256**, 71 (1996).
[40] M. N. R. Ashfold, D. W. Chandler, C. C. Hayden, R. I. McKay, and A. J. R. Heck, Chem. Phys. Lett. **201**, 237 (1995).
[41] H. Li and W. Kong, J. Chem. Phys. **107**, 3774 (1997).
[42] T. Ebata, A. Okazaki, Y. Inokuchi, and N. Mikami, J. Mol. Struct. **352/353**, 533 (1995).
[43] M. D. Wheeler, I. R. Lambert, and M. N. R. Ashfold, Chem. Phys. Lett. **229**, 285 (1994).
[44] M. A. Buntine, D. W. Chandler, and C. C. Hayden, J. Chem. Phys. **102**, 2718 (1995).
[45] J. Ishii, K. Uehara, and K. Tsukiyama, J. Chem. Phys. **102**, 9174 (1995).
[46] J. Geng, T. Kobayashi, and M. Takami, Chem. Phys. Lett. **266**, 290 (1997).
[47] E. F. McCormack, S. T. Pratt, P. M. Dehmer, and J. L. Dehmer, J. Chem. Phys. **102**, 4740 (1995).
[48] E. F. McCormack, S. T. Pratt, P. M. Dehmer, and J. L. Dehmer, Aust. J. Phys. **49**, 445 (1996).
[49] S. Williams, R. N. Zare, and L. A. Rahn, J. Chem. Phys. **101**, 1072 (1994).
[50] S. Williams, E. A. Rohlfing, L. A. Rahn, and R. N. Zare, J. Chem. Phys. **106**, 3090 (1997).
[51] S. Williams, J. D. Tobiason, J. R. Dunlop, and E. A. Rohlfing, J. Chem. Phys. **102**, 8342 (1995).
[52] F. Di Teodoro and E. F. McCormack, Phys. Rev. A **57**, 162 (1998).
[53] See, for example, J. F. Reintjes, *Nonlinear Optical Parametric Processes in Liquids and Gases* (Academic, New York, 1984); H. J. Eichler, P. Gunter, and D. W. Pohl, *Laser-Induced Dynamic Gratings* (Springer-Verlag, Berlin, 1986); IEEE J. Quantum Electron. **QE-22**, 1 (1986).
[54] T. K. Yee and T. K. Gustafson, Phys. Rev. A **18**, 1597 (1978).
[55] S. A. J. Druet and J. P. E. Taran, Prog. Quantum Electron. **7**, 1 (1981).
[56] Y. Prior, IEEE J. Quantum Electron. **QE-20**, 37 (1984).
[57] R. Trebino, Phys. Rev. A **38**, 2921 (1988).
[58] U. Fano, Phys. Rev. **124**, 1866 (1960).
[59] H. Freidrich, *Theoretical Atomic Physics* (Springer, Berlin, 1991).
[60] G. Herzberg, *Molecular Spectra and Molecular Structure, I. Spectra of Diatomic Molecules* (Van Nostrand Reinhold, Princeton, 1950).
[61] S. N. Dixit, D. L. Lynch, and V. McKoy, Phys. Rev. A **32**, 1267 (1985).
[62] F. M. Phelps, III, *MIT Wavelength Tables 2* (MIT Press, Cambridge, MA, 1982).
[63] J. M. Grochocinski, M. A. thesis, Bryn Mawr College, 1997.
[64] R. Engleman, P. E. Rouse, H. M. Peek, and V. D. Baiamonte, Los Alamos Scientific Laboratory Report LA-4364, 1970.
[65] R. C. Hilborn, Am. J. Phys. **50**, 985 (1982).
[66] L. G. Piper and L. M. Cowles, J. Chem. Phys. **85**, 2419 (1986).